Effect of Temperature Variation on Bayesian Anomaly Detection in Model Bridge Experiments

Yuki Hirate
Graduate Student, Dept. of Civil and Earth Resources Engineering, Kyoto University, Kyoto, Japan

Chul-Woo Kim
Professor, Dept. of Civil and Earth Resources Engineering, Kyoto University, Kyoto, Japan

ABSTRACT: In the long-term structural health monitoring (SHM) of bridges, seasonal changes such as temperature affect the vibration characteristics of bridges. This study aims to investigate the influences of temperature changes on the vibration characteristics of bridges through in-house moving vehicle experiments on an artificially damaged model bridge. Instead of conventional modal parameters, the system matrix of a state space model is proposed as a damage-sensitive feature. Considering uncertainties in vibration data and the state space model, the system matrix is identified by Bayesian inference in terms of Bayesian system identification. Changes in the damage-sensitive feature under artificial damage are detected using the Bayes factor (BF) as a Bayesian hypothesis test.

1. INTRODUCTION

The importance of maintenance and management of bridge stock for safe and long-term use is becoming increasingly important worldwide. In Japan as an example, the bridge condition assessment for the maintenance and management of bridge stock is based on visual inspections despite its time and labor-consuming processes.

As an alternative for visual inspection, structural health monitoring (SHM) of bridges utilizing sensor information has been investigated. Different from the visual inspection, it is expected that sensor information could provide objective information as it is directly relevant to physical quantities such as strain, displacement, acceleration, etc. Among these sensors, utilizing accelerometers has been popular in SHM campaign of bridges because they are easy to install and do not require a fixed point (Farrar et al. 1994; Magalhaes et al. 2012; Kim et al. 2013). In particular, long-term monitoring, which focuses on changes in vibration characteristics over a long period of time, is also gaining more attention as a practical SHM for bridges. However, seasonal changes in the vibration characteristics of bridges in long-term vibration monitoring are well-known phenomena and are mainly caused by temperature changes. It is therefore necessary to have a better understanding of the effects of temperature variations on bridge vibration characteristics.

The aim of this study is thus to investigate the effects of temperature changes on the vibration characteristics of bridges by means of in-house moving vehicle experiments on an artificially damaged model bridge. The modal characteristics of the model bridge were identified from the measured accelerations using the stochastic subspace identification (SSI) method (Van Overschee and De Moor 1996) and changes in vibration characteristics were investigated. Instead of conventional modal parameters, the system matrix of a state space model is proposed as a damage-sensitive feature. Considering uncertainties in vibration data and the state space model, the system matrix is identified by Bayesian inference in terms of Bayesian system identification (Goi and Kim 2019). Changes in the damage-sensitive feature under artificial damage are detected using the Bayes factor (BF) (Kass and Raftery 1995) as a Bayesian hypothesis test.

2. BAYESIAN ANOMALY DETECTION WITH VAR MODEL

2.1. Vector autoregressive model of dynamic system

Assuming that a discrete acceleration time series with *m* degrees of freedom is measured for a bridge, and consider a column vector $\boldsymbol{y}_k \in \mathbb{R}^{m\times 1}$ that consists of these time series in which *k* denotes the time step of the discrete-time series and *m* is the number of observation points or the number of sensors. It is known that the acceleration time series $\boldsymbol{y}_k$ can be approximated by a vector autoregressive (VAR) process with an appropriate model order *p* as Eq. (1). The mode frequency, mode damping, and mode shape can be identified from the coefficient matrix of the VAR model (Kim et al. 2012).

$$\boldsymbol{y}_k = \sum_{i=1}^{p} \boldsymbol{\alpha}_i \boldsymbol{y}_{k-i} + \boldsymbol{e}_k \tag{1}$$

where $\boldsymbol{\alpha}_i \in \mathbb{R}^{m\times m}$ is the *i*-th order autoregressive coefficient matrix and $\boldsymbol{e}_k \in \mathbb{R}^{m\times 1}$ is the time series of white Gaussian noise vectors. To simplify the discussion, let $\mathbf{W} = [\boldsymbol{\alpha}_1, \dots, \boldsymbol{\alpha}_p] \in \mathbb{R}^{m\times mp}$ and rewrite Eq. (1) as Eq. (2).

$$\begin{aligned} \boldsymbol{y}_k &= \mathbf{W}\{\boldsymbol{y}_{k-1} \quad \cdots \quad \boldsymbol{y}_{k-p}\}^T + \boldsymbol{e}_k \\ &= \mathbf{W}\boldsymbol{\phi}_k + \boldsymbol{e}_k \end{aligned} \tag{2}$$

where $\boldsymbol{\phi}_k \in \mathbb{R}^{mp\times 1}$ is the column vector of $\boldsymbol{y}_{k-1}, \dots, \boldsymbol{y}_{k-p}$ arranged vertically. Let $\boldsymbol{\Sigma}$ be the covariance matrix of the noise vector $\boldsymbol{e}_k$, the probability density function (PDF) of $\boldsymbol{y}_k$ is expressed as follows.

$$\mathrm{p}(\boldsymbol{y}_k|\boldsymbol{\phi}_k, \boldsymbol{W}, \boldsymbol{\Sigma}) = \mathcal{N}(\boldsymbol{y}_k|\boldsymbol{W}\boldsymbol{\phi}_k, \boldsymbol{\Sigma}) \tag{3}$$

where $\mathrm{p}(\cdot\,|\,\cdot)$ represents the conditional probability density function and $\mathcal{N}(\boldsymbol{x}|\boldsymbol{\mu}, \boldsymbol{\Sigma})$ stands the PDF of $\boldsymbol{y}_k$ following the vector Gaussian distribution with expectation $\mathbf{W}\boldsymbol{\phi}_k$ and covariance matrix $\boldsymbol{\Sigma}$.

Consider the problem of estimating the regression coefficients $\boldsymbol{W}$ and the covariance $\boldsymbol{\Sigma}$ of the regression error from the observed values of the target variable $\boldsymbol{y}$ using Bayes' theorem. Let *n* target variables $\boldsymbol{y}_1, \dots, \boldsymbol{y}_n$ correspond to inputs $\boldsymbol{\phi}_1, \dots, \boldsymbol{\phi}_n$, and consider the data set $\mathbf{Y} = [\mathbf{y}_1, \dots, \mathbf{y}_n] \in \mathbb{R}^{m\times n}$ and $\boldsymbol{\phi} = [\boldsymbol{\phi}_1, \dots, \boldsymbol{\phi}_n] \in \mathbb{R}^{mp\times n}$ for simplicity. Eq. (3) leads to Eq. (4) for the parameters $\boldsymbol{W}$ and $\boldsymbol{\Sigma}$ are obtained. The conditional PDF in Eq. (3) is the likelihood function of **Y** for parameters **W** and **Σ**. According to Bayes theorem, the PDF of **W** and **Σ** conditioned to **Y** is estimate.

$$\begin{aligned} &\mathrm{p}(\mathbf{Y}|\mathbf{W}, \boldsymbol{\Sigma}) \\ &= \mathrm{p}(\boldsymbol{\phi}_{p+1}) \prod_{k=p+1}^{n} \mathcal{N}(\boldsymbol{y}_k|\mathbf{W}\boldsymbol{\phi}_k, \boldsymbol{\Sigma}) \end{aligned} \tag{4}$$

2.2. Optimal model of VAR process

The optimal order of the VAR process is determined using the Bayesian Information Criterion (BIC). The acceleration of the healthy bridge is used as reference data and the acceleration of the damaged bridge as test data. The BIC of the reference data Y_r is expressed as Eq. (5).

$$\begin{aligned} BIC &= -2ln\mathrm{p}\left(Y_r\middle|\widehat{\boldsymbol{W}}_r, \widehat{\boldsymbol{\Sigma}}_r\right) \\ &+ \left(m^2 p + \frac{m(m+1)}{2}\right) ln\left(\Sigma_{i=1}^{l} n_i - p\right) \end{aligned} \tag{5}$$

where $\widehat{\boldsymbol{W}}_r$ and $\widehat{\boldsymbol{\Sigma}}_r$ are the maximum likelihood estimators that maximize the likelihood function $\mathrm{p}(Y_r|\boldsymbol{W}, \boldsymbol{\Sigma})$, *m* is the number of sensors, l is the length of acceleration time series and n_i is the length of all data sets. BIC is calculated starting from *p* =1, and the *p* with the smallest BIC value is adopted as the optimal VAR order.

2.3. Bayesian Inference

The parameters $\boldsymbol{W}$ and $\boldsymbol{\Sigma}$ are denoted as the regression parameters. As mentioned in Section 2.1, the mode frequencies, mode damping, and mode shapes are identified from the coefficient matrix $\boldsymbol{W}$ of the VAR model. Therefore, the regression parameter $\boldsymbol{W}$ is used as the damage-sensitive feature, and its posterior distribution is obtained using Bayes' theorem as follows.

$$\begin{aligned} &\mathrm{P}(\boldsymbol{W}, \boldsymbol{\Sigma}|\boldsymbol{Y}) \\ &= \mathrm{p}(\boldsymbol{Y}|\boldsymbol{W}, \boldsymbol{\Sigma})\mathrm{p}(\boldsymbol{W}, \boldsymbol{\Sigma})\mathrm{p}(\boldsymbol{Y})^{-1} \end{aligned} \tag{6}$$

where $\mathrm{p}(\boldsymbol{W}, \boldsymbol{\Sigma})$ on the right-hand side is the prior probability density function of the regression parameters. On the other hand, $\mathrm{p}(\boldsymbol{W}, \boldsymbol{\Sigma}|\boldsymbol{Y})$ on the left side represents the posterior distribution of the

regression parameters obtained conditional on the observations. Bayesian damage detection focuses on the ratio of the posterior distribution in terms of Bayesian hypothesis testing, which is described in Section 2.4. The process of calculating the posterior distribution is called Bayesian inference.

In Bayesian inference, it is known that a closed solution to the probability density function of the posterior distribution can be obtained by assuming a prior distribution called a conjugate prior distribution (Bishop 2006). In addition, from the viewpoint of numerical analysis, the conjugate prior distribution is known to be effective in terms of computational efficiency for high-speed calculations for in-service damage detection. For the likelihood function in Eq. (4), the conjugate prior distribution of the regression parameters is known to be a matrix-normal inverse Wishart distribution defined by the following Eq. (7) (Dzunic et al. 2017).

$$\begin{aligned}&\mathrm{P}(\boldsymbol{W},\boldsymbol{\Sigma})\\&=\mathcal{MN}(\boldsymbol{W}|\boldsymbol{M},\boldsymbol{\Sigma},\boldsymbol{L}^{-1})\mathcal{IW}(\boldsymbol{\Sigma}|\boldsymbol{\Psi},\boldsymbol{\nu})\end{aligned} \tag{7}$$

where $\mathcal{MN}(\mathbf{W}|\mathbf{M},\boldsymbol{\Sigma},\mathbf{L}^{-1})$ and $\mathcal{IW}(\boldsymbol{\Sigma}|\boldsymbol{\Psi},\nu)$ are probability density functions that follow a matrix normal distribution and an inverse Wishart distribution, respectively, and are defined as follows.

$$\begin{aligned}&\boldsymbol{\mathcal{MN}}(\boldsymbol{W}|\boldsymbol{M},\boldsymbol{\Sigma},\boldsymbol{L}^{-1})=\\&(\boldsymbol{2\pi})^{-(\boldsymbol{mp}\times\boldsymbol{m})/2}\left|\boldsymbol{L}^{-1}\right|^{-\boldsymbol{m}/2}|\boldsymbol{\Sigma}|^{-\boldsymbol{mp}/2}\\&\times\boldsymbol{exp}\left\{-\frac{\mathbf{1}}{\mathbf{2}}\boldsymbol{tr}[\boldsymbol{L}(\boldsymbol{W}-\boldsymbol{M})^{\boldsymbol{T}}\boldsymbol{\Sigma}^{-\mathbf{1}}(\boldsymbol{W}-\boldsymbol{M})]\right\}\\&\boldsymbol{\mathcal{IW}}(\boldsymbol{\Sigma}|\boldsymbol{Q},\boldsymbol{\nu})\end{aligned} \tag{8}$$

$$\begin{aligned}&=\boldsymbol{2}^{-\boldsymbol{\nu m}/2}\boldsymbol{\Gamma}_{\boldsymbol{m}}\left(\frac{\boldsymbol{\nu}}{\mathbf{2}}\right)|\boldsymbol{Q}|^{\boldsymbol{\nu}/2}|\boldsymbol{\Sigma}|^{-(\boldsymbol{\nu}+\boldsymbol{m}+\mathbf{1})/2}\\&\times\boldsymbol{exp}\left\{-\frac{\mathbf{1}}{\mathbf{2}}\boldsymbol{tr}[\boldsymbol{Q}\boldsymbol{\Sigma}^{-\mathbf{1}}]\right\}\end{aligned} \tag{9}$$

The parameters $\mathbf{M}\in\mathbb{R}^{m\times mp}$, $\mathbf{L}\in\mathbb{R}^{mp\times mp}$, $\boldsymbol{Q}\in\mathbb{R}^{m\times m}$ and $\nu\in\mathbb{R}$ are called the hyperparameters. The probability density function of the posterior distribution is known to be expressed as follows.

$$\begin{aligned}&\mathrm{P}(\boldsymbol{W},\boldsymbol{\Sigma}|\boldsymbol{Y})\\&=\mathcal{MN}\left(\boldsymbol{W}|\boldsymbol{M}',\boldsymbol{\Sigma},\boldsymbol{L}'^{-1}\right)\mathcal{IW}(\boldsymbol{\Sigma}|\boldsymbol{Q}',\boldsymbol{\nu}')\end{aligned} \tag{10}$$

The hyperparameters $\mathbf{M}'$, $\mathbf{L}'$, $\boldsymbol{Q}'$and ν'in Eq. (10) are calculated as follows.

$$\mathbf{L}'=\mathbf{L}+\sum_{k=p+1}^{n}\boldsymbol{\phi}_k\boldsymbol{\phi}_k{}^{\mathrm{T}} \tag{11}$$

$$\mathbf{M}'=\left(\mathbf{ML}+\sum_{k=p+1}^{n}\boldsymbol{y}_k\boldsymbol{\phi}_k{}^{\mathrm{T}}\right)\mathbf{L}'^{-1} \tag{12}$$

$$\nu'=\nu+n-p \tag{13}$$

$$\begin{aligned}\boldsymbol{Q}'=\boldsymbol{Q}+\mathbf{Y}\sum_{k=p+1}^{n}\boldsymbol{y}_k\boldsymbol{y}_k{}^{\mathrm{T}}+\mathbf{MLM}^{\mathrm{T}}\\-\mathbf{M}'\mathbf{L}'\mathbf{M}'^{\mathrm{T}}\end{aligned} \tag{14}$$

The hyperparameters shown in Eqs. (11), (12), (13) and (14) can be updated sequentially using observed data. However, in the first step of the sequential algorithm, the observed values are not available, and it is common to use non-informative prior distribution (Jeffreys 1946) as the prior distribution of the unknown regression parameters. To represent the non-informative prior in the first step of the sequential update, the initial values of the hyperparameters are set as $\mathbf{L}=\mathbf{O}$, $\nu=0$, and $\boldsymbol{Q}=\mathbf{O}$.

2.4. Bayes Hypothesis Tests with Bayes Factors

The Bayes factor (BF) is used in Bayesian hypothesis testing, where the BF is defined as the ratio of the likelihood functions. Let $\boldsymbol{Y}$ be the observed data set, and $\boldsymbol{\theta}=(\boldsymbol{W},\boldsymbol{\Sigma})$ be the regression parameter. The likelihood function for $\mathrm{H_k}$ is defined as Eq. (15).

$$\mathrm{p}(\boldsymbol{Y}|\mathrm{H_k})=\int\mathrm{p}(\boldsymbol{Y}|\boldsymbol{\theta},\mathrm{H_k})\mathrm{p}(\boldsymbol{\theta}|\mathrm{H_k})\,d\boldsymbol{\theta} \tag{15}$$

where $\mathrm{p}(\boldsymbol{Y}|\boldsymbol{\theta},\mathrm{H_k})$ and $\mathrm{p}(\boldsymbol{\theta}|\mathrm{H_k})$ are the likelihood function and prior distribution under the hypothesis $\mathrm{H_k}$, respectively. The posterior distribution under the hypothesis $\mathrm{H_k}$ is expressed as follows by Bayes theorem.

$$\mathrm{p}(\mathrm{H_k}|\boldsymbol{Y})=\mathrm{p}(\boldsymbol{Y}|\mathrm{H_k})\mathrm{p}(\mathrm{H_k})\mathrm{p}(\boldsymbol{Y})^{-1} \tag{16}$$

Two hypotheses, the null hypothesis $\mathrm{H_0}$ and the alternative hypothesis $\mathrm{H_1}$, are defined as the hypothesis $\mathrm{H_k}$. The null hypothesis $\mathrm{H_0}$ is "the statistical model that observed values follow is identical to that of the bridge in a healthy

condition. Since it is difficult to model the prior distribution of the alternative hypothesis H_1, it is assumed for convenience that "the priori information is uncertain about the statistical model that the observed values follow". The ratio of the posterior distribution, Bayes factor (BF), for each hypothesis obtained from Eq. (16) is expressed as follows.

$$\frac{p(H_1|\boldsymbol{Y})}{p(H_0|\boldsymbol{Y})} = \frac{p(H_1)}{p(H_0)} \frac{p(\boldsymbol{Y}|H_1)}{p(\boldsymbol{Y}|H_0)} \tag{17}$$

From Eq. (17), the ratio of the posterior distribution can be expressed as the ratio of the prior distribution and the likelihood function. Assuming that the probabilities of the null hypothesis H_0 and the alternative hypothesis H_1 are equal, i.e., $p(H_0) = p(H_1)$, the BF can be expressed as the ratio of the likelihood function. In other words, the BF is an indicator to evaluate whether the dataset **Y** follows the null hypothesis H_0 or the alternative hypothesis H_1. Kass and Raftery (1995) proposed that the BF shown in Eq. (18) is considered on a natural logarithm scale, and if $2lnB$ is greater than 0, the evidence is strong that there is "very strong" evidence to reject the null hypothesis.

$$BF = 2lnB = 2ln\left(\frac{p(\boldsymbol{Y}|H_1)}{p(\boldsymbol{Y}|H_0)}\right) \tag{18}$$

3. IN-HOUSE EXPERIMENT

3.1. Vibration and damage experiment

Moving vehicle experiments were conducted with a model bridge of a simple supported H-shaped steel girder. The span length of the bridge is 5400 mm, the width is 287 mm, and the depth is 66 mm.

The detail of the model bridge, sensor placement, and artificial damage are shown in Figure 1. The supports denoted Ab1 and Ab2 in Figure 1 adopt pin and roller supports respectively. In the experiment, accelerations, displacement, and surface temperature were measured. The triaxial accelerometers, M-A552AC10 (Epson), were placed on the bottom surface of the bridge at five points (from A1 to A5). Both contact-type displacement transducer (Tokyo Measuring Instruments Lab.) and laser displacement transducer, IL-065 (Keyence), were used. A contact-type displacement transducer was installed span center of the bridge, denoted as D1 in Figure 1, and the laser displacement transducers were installed at the roller support Ab2 in the longitudinal direction that is denoted L1 and L2 in Figure 1. The laser displacement transducers were deployed to measured longitudinal movement of the bridge during temperature changes. Thermocouples (Tokyo Measuring Instruments Lab.) were placed on the underside of the flooring with equal spacing at six points (from T1 to T6) spaced in 4 equal divisions of the span length. For measuring displacement, the NR-600 (Keyence) was used as the data logger and for measuring surface temperature, the TDS-530 (Tokyo Measuring Instruments Lab.) was used.

In damage experiments, the bridge was artificially damaged in the center of the span and at the ends, as shown in Figure 1. The damage was created by applying three slits in the middle of the span, as shown in Figure 2 a), and the flanges of the bridge ends were trimmed off in a triangular shape, as shown in Figure 2 c). The damage was reinforced as shown in Figure 2 b) and d) and deemed a healthy state. As damage scenarios, DMG0, DGM1, DGM2, and DMG12 denote the healthy state, the damage state with artificial slits at the center of the span, the damage state with trimmed web plate at the end of the bridge, and the damage state with both artificial slits and trimmed plate.

The flexural rigidities of the bridge under DMG0, DGM1, DGM2, and DMG12 scenarios were $1.4777\text{E}+11\ (\text{N}\cdot mm^2)$, $1.2611\text{E}+11\ (\text{N}\cdot mm^2)$, $1.4354\text{E}+11\ (\text{N}\cdot mm^2)$, $1.2617\text{E}+11\ (\text{N}\cdot mm^2)$, respectively. It is noted that the flexural rigidity of the bridge was not reduced due to DMG2, i.e., only a 3% reduction of the flexural rigidity, while a 15% reduction of the flexural rigidity due to DMG1 was observed.

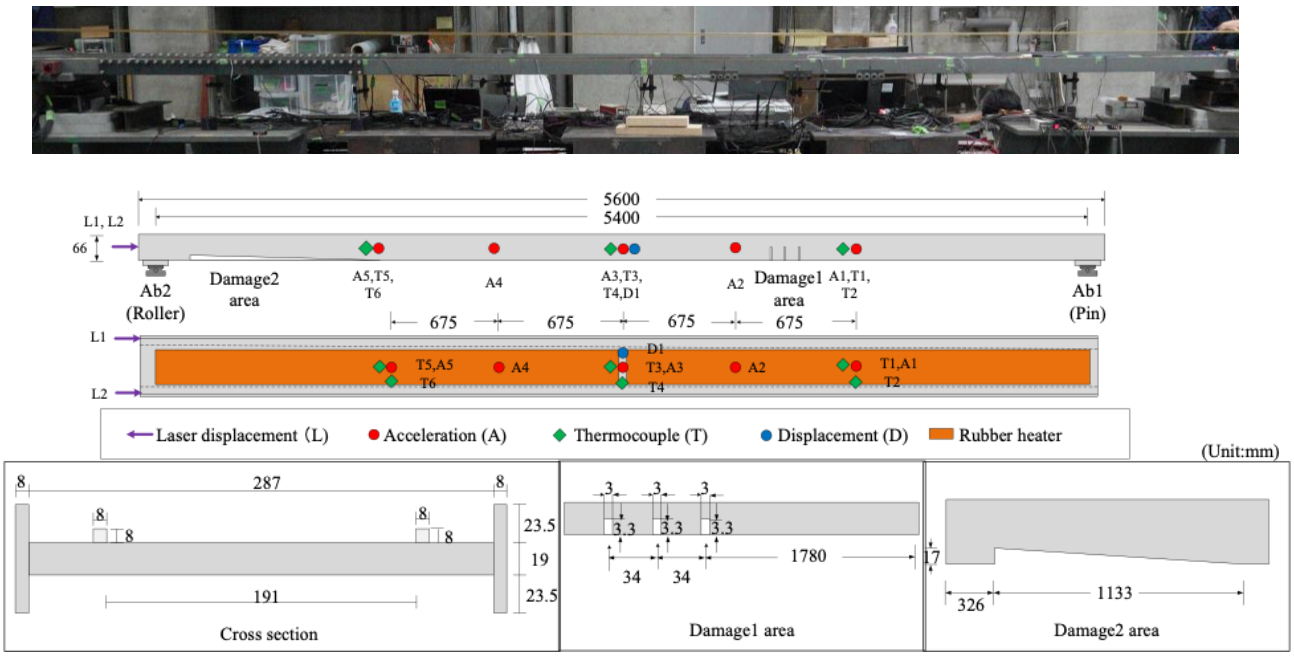

Figure 1: Model bridge, position of the sensors, and artificial damage.

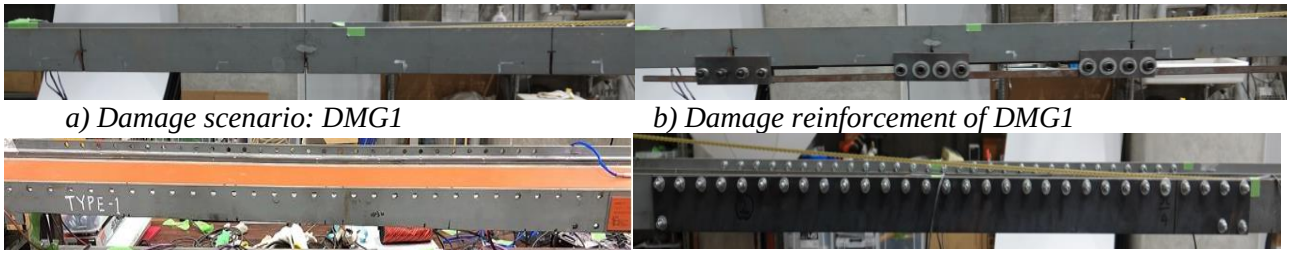

a) Damage scenario: DMG1 *b) Damage reinforcement of DMG1*

c) Damage scenario: DMG2 *d) Damage reinforcement of DMG2*

Figure 2: Artificial damages and healthy states subject to damage reinforcement.

Rubber heaters were used to vary the surface temperature of the bridge. During the moving vehicle experiment on the bridge, the surface temperature was set at 25℃, 35℃, 45℃, and 55℃. These temperature scenarios are denoted as T25, T35, T45, and T55.

In the moving vehicle experiments on the model bridge, the weight of the model vehicle was approximately 135N. The vehicle speed was determined to be consistent with the dimensionless parameter α shown in Eq. (19) for both the model bridge and an actual bridge with a span length of 36 m.

$$\alpha = \frac{v}{2fL} \tag{19}$$

where v denotes the vehicle speed (m/s), f is the natural frequency of the first bending mode of the bridge (Hz), and L is the span length (m).

In this experiment, the model vehicle was operated at a speed of 0.84 m/s, equivalent to 20 km/h on the actual bridge. The number of trials for each run was 20 for all scenarios. The direction of travel was between Ab1 and Ab2 in Figure 1, with one-way being considered as one trial and the sampling frequency was 200 Hz.

The total number of experiments is 320 trials: four temperature scenarios, four damage scenarios, and 20 runs of the moving vehicle test. Hereafter, the notation of the experiment scenario is defined as "(DMGn, Tm)" in which n denotes the ID of damage scenarios, i.e., 0, 1, 2, or 12, and m denotes the planned temperature.

Table 1: Identified Frequency at T25(Hz).

Bending Mode	DMG0	DMG1	DMG2	DMG12
1st	3.49	3.66	3.45	3.41
2nd	9.73	9.47	9.56	9.38
3rd	23.18	22.75	22.63	22.50

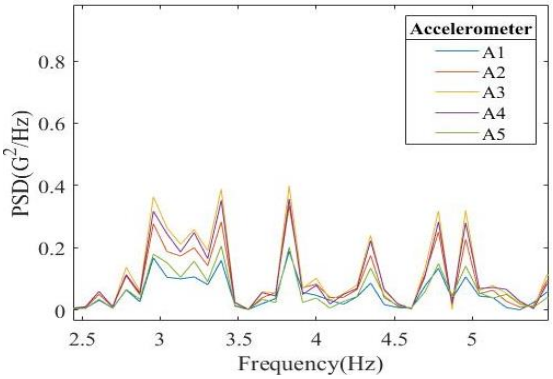

Figure 3: PSD of acceleration (DMG0, T25).

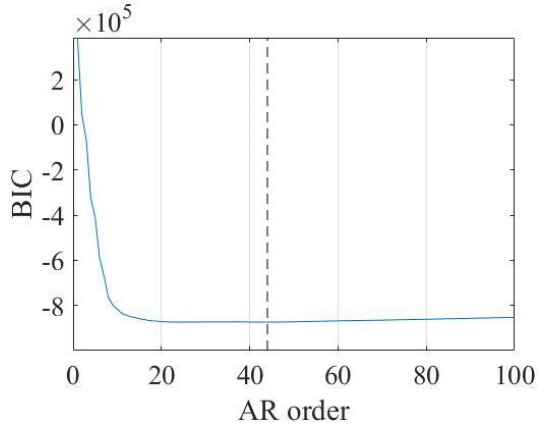

Figure 4: Optimal AR order by BIC.

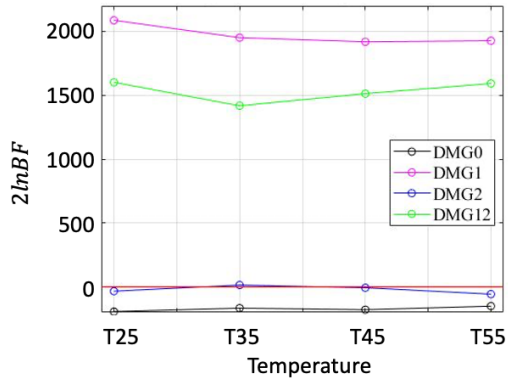

Figure 5: BF (DMG0, T25 is reference data.)

3.2. Vibration characteristics of model bridge

Vibration characteristics were identified by the SSI utilizing accelerations. The mean values of the identified frequencies at 25℃ are summarized in Table 1, which shows changes in the natural vibration frequencies associated with the damage state. Frequencies of the second and third bending modes decreased due to the damage states (DMG1, DMG2, DMG12). On the other hand, the frequency of the first bending mode increased from DMG0 to DMG1 despite the damage.

One reason for the increasing trend of the first bending frequency due to damage in the DMG1 scenario is in difficulty to select the proper frequency relevant to the first bending mode as shown in the PSD curve in Figure 3. The PSD curve shows multiple peaks around the first bending frequency, and the cause of the increase in the frequency of the first bending mode was the extraction of a vibration mode other than the first bending mode. The cause of appearing multiple peaks could be the influence of the vehicle-bridge interaction (Chang et al. 2014).

4. ANOMALY DETECTION USING BAYES FACTOR

As discussed in Section 3.2, it was found that sensitivity to damage varies depending on the vibration mode. However, it was not easy to determine the vibration modes that were sensitive to damage beforehand. Therefore, the coefficient matrix of the VAR model is used as a damage-sensitive feature, and the Bayesian hypothesis test with BF is carried out as anomaly detection.

4.1. Variations of BF under temperature changes

In order to investigate the feasibility of damage detection under changing temperatures, the change in BF is examined. First, the optimal model order of the VAR model is determined using the BIC in Eq. (5). Figure 4 shows BIC with respect to the model order of the VAR model, and the minimum BIC was observed at $p = 44$. $p = 44$ is thus deemed the optimal autoregressive order.

BFs estimated considering the optimal autoregressive order, $p = 44$, are illustrated in Figure 5 in which data from (DMG0, T25) is used

as reference data. Figure 5 shows that the effect of temperature changes on the BF was small in DMG0 and DMG2 scenarios, while the BFs of DMG1 and DMG12 are affected by the temperature changes. However, in terms of damage detection, the BFs of DMG1 and DMG12 are clearly higher than DMG0 even taking temperature effects into account.

Considering real-world applications, the reference BF could be estimated from at least one year of monitoring data so that seasonal changes can be included in the reference BF. Therefore, the reference BF is estimated using all data of the DMG0 considering four temperature scenarios.

Figure 6 shows the plot of BFs of different damage scenarios under different temperatures. It is observed that the BFs of DMG1 and DMG12 scenarios clearly indicate "very strong" evidence to reject the null hypothesis, i.e., healthy state, although temperature changes influence the BF. For DMG2, where the reduction in bending stiffness is negligible even after trimming the web plates at the bridge ends, the BF shows 'very weak' evidence to reject the null hypothesis, as expected.

5. CONCLUSIONS

This study investigates the effects of temperature changes on the vibration characteristics of bridges by means of in-house moving vehicle experiments on an artificially damaged model bridge. Changes in the damage-sensitive feature under artificial damage and varying temperatures using are also investigated using the Bayes factor (BF) as a Bayesian hypothesis test.

Observations demonstrated that temperature changes affect the BF when the reduction of flexural rigidity is big. However, for the damaged bridge under damage at the span center resulted in around a 15% reduction of flexural rigidity BFs showed clear changes even taking temperature effects into account. In other words, the BF of the damaged bridge clearly indicates "very strong" evidence to reject the null hypothesis, i.e., a healthy state, although temperature changes have some effect on the BF.

6. ACKNOWLEDGMENTS

A part of this work is supported by JSPS Bilateral joint research projects, Grant No. JPJSBP120217405, and the Japanese Society for the Promotion of Science (JSPS) Grant-in-Aid for Scientific Research (B) under project No.22H01576. Those technical and financial supports are gratefully acknowledged.

7. REFERENCES

Bishop, C.M. (2006). “Pattern recognition and machine learning.” *New York: Springer*.

Chang, K.C., Kim, C.W. and Borjigin, S. (2014). “Variability in bridge frequency induced by a parked vehicle.” *Smart Structures and Systems*, An Int J., 13(5): 755-773.

Dzunic, Z., Chen, J.G., Mobahi, H., Büyüköztürk, O. and Fisher, J.W. (2017). “A Bayesian state-space approach for damage detection and classification.” *Mech. Syst. Signal Process*, 96: 239–259.

Farrar, C.R., Baker, W.E., Bell, T.M., Cone, K.M., Darling, T.W., Duffey, T.A., Eklund, A. and Migliori, A. (1994). “Dynamics characterization and damage detection in the I-

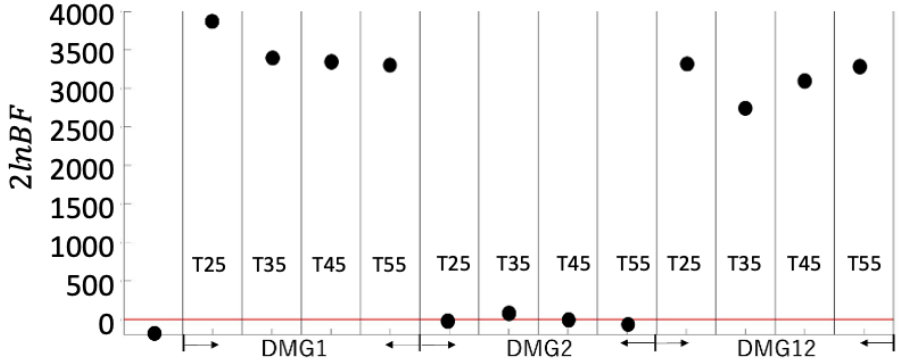

Figure 6: BF (All data of four temperature scenarios of DMG0 are reference data).

40 Bridge over the Rio Grande." *LANL report*: LA-12767-MS.

Goi, Y. and Kim, C.W. (2017). "Damage detection of a truss bridge utilizing a damage indicator from multivariate autoregressive model*." Journal of Civil Structural Health Monitoring*, 7(2): 153-162.

Goi, Y. and Kim, C.W. (2019). "Vibration-based damage detection of steel bridges using Bayesian hypothesis testing." *Proceedings of the 29th European Safety and Reliability Conference*, Hannover, Germany.

Jeffreys, H. (1946). "An invariant form for the prior probability in estimation problems." *Proceedings of the Royal Society of London*, 186: 453–461.

Kass, R. and Raftery, A. (1995). "Bayes Factors," *J of the American Statistical Association*, 90(430): 773–795.

Kim, C.W., Kawatani, M. and Hao, J. (2012). "Modal parameter identification of short span bridges under a moving vehicle by means of multivariate AR model." *Structure and Infrastructure Engineering*, 8(5): 459-472.

Kim, C.W., Isemoto, R., Sugiura, K., and Kawatani, M. (2013) "Structural fault detection of bridges based on linear system parameter and MTS method." *J. of JSCE*, JSCE, 1(1): 32-43.

Ministry of Land, Infrastructure, Transport and Tourism (2020). "*Road Maintenance Annual Report".*

Magalhaes, F., Cunha, A. and Caetano E. (2012). "Vibration based structural health monitoring of an arch bridge: From automated OMA to damage detection" *Mech. Syst. Signal Process.*, 28: 212-228.

Nair, K.K., Kiremidjian, A.S. and Law, K.H. (2006). "Time series-based damage detection and localization algorithm with application to the ASCE benchmark structure." *J. Sound Vib.*, 291: 349-368.

Van Overschee, P. and De Moor, B. (1996). "Subspace identification for linear systems." *Kluwer Academic Publishers*.